

Theoretical Limit of Low Temperature Subthreshold Swing in Field-Effect Transistors

Arnout Beckers¹, Farzan Jazaeri¹, and Christian Enz¹, *Fellow, IEEE*

Abstract—This letter reports a temperature-dependent limit for the subthreshold swing in MOSFETs that deviates from the Boltzmann limit at deep-cryogenic temperatures. Below a critical temperature, the derived limit saturates to a value that is independent of temperature and proportional to the characteristic decay of a band tail. The proposed expression tends to the Boltzmann limit when the decay of the band tail tends to zero. Since the saturation is universally observed in different types of MOSFETs (regardless of dimension or semiconductor material), this suggests that an intrinsic mechanism is responsible for the band tail.

Index Terms—Band tail, cryogenic, MOSFET, modeling, subthreshold slope, subthreshold swing.

I. INTRODUCTION

THE Boltzmann limit of the subthreshold swing in FETs, $SS = (k_B T/q) \ln 10$, predicts at room temperature the well-known ≈ 60 mV/dec, and at deep-cryogenic temperatures ($< \approx 50$ K) an almost ideal, step-like switch ($k_B T/q$ is the thermal voltage). However, the measurements in FETs at deep-cryogenic temperatures reach merely ≈ 11 instead of 0.8 mV/dec at 4.2 K [1]–[6], ≈ 9 mV/dec instead of 20 μ V/dec at 100 mK [7], and ≈ 7 mV/dec instead of 4 μ V/dec at 20 mK [8]. As shown in Fig. 1, this degradation is measured in structurally different FETs, operating in subthreshold at both low and high drain-source voltage (V_{DS}) and for various technologies: mature and advanced bulk and FDSOI (Fully-Depleted Silicon-On-Insulator) MOSFETs [4]–[14], FinFETs [15], [16], gate-all-around Si nanowire FETs [17], junctionless FETs [18], [19], SiGe FETs [20], InP HEMTs [21], SiC FETs [22], etc. Figure 1 highlights this measured trend, deviating from the Boltzmann limit below a critical temperature, and then saturating to a value depending on the technology. The difference between the measured SS and the Boltzmann limit is referred to as excess SS . The additional power that the FET consumes at deep-cryogenic temperatures due to the excess SS is a crucial metric for the realization of quantum processors in silicon [23]–[30] and for assessing the

Manuscript received December 2, 2019; revised December 23, 2019; accepted December 26, 2019. This work was supported by the European Union’s Horizon 2020 Research and Innovation Programme MOS-Quito (MOS-based Quantum Information Technology) under Grant 688539. The review of this letter was arranged by Editor V. Moroz. (Corresponding author: Arnout Beckers.)

The authors are with the Integrated Circuits Laboratory (ICLAB), Ecole Polytechnique Fédérale de Lausanne (EPFL), 2000 Neuchâtel, Switzerland (e-mail: arnout.beckers@epfl.ch).

Color versions of one or more of the figures in this letter are available online at <http://ieeexplore.ieee.org>.

Digital Object Identifier 10.1109/LED.2019.2963379

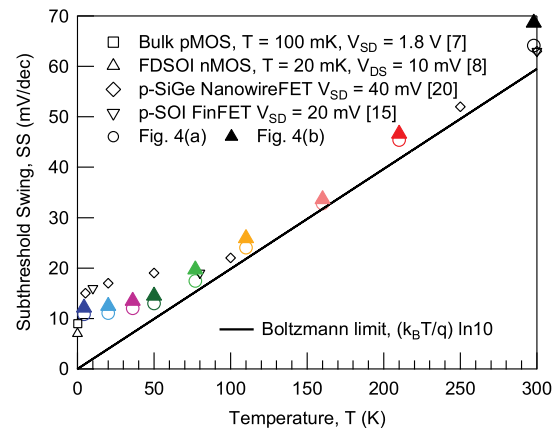


Fig. 1. Saturating $SS(T)$ measured in different FET technologies deviating from the Boltzmann limit. Colored markers are obtained from our measurements in Figs. 4(a) and 4(b) at $I_{DS} = 100$ pA and 1 nA, respectively. All devices have gate lengths in the μ m-range.

benefits of temperature scaling as an alternative to traditional scaling [9], [10], [31].

It is simply not possible to explain the saturation of $SS(T)$ using the Boltzmann limit. Indeed, the Boltzmann limit is linear in T . Its slope versus T in the plot in Fig. 1 is proportional to the slope factor m_0 [$SS = m_0(k_B T/q) \ln 10$], where $m_0 = 1 + C_{depl}/C_{ox}$, with C_{ox} the gate-oxide capacitance, and C_{depl} the depletion capacitance. The slope factor m_0 is limited to 2 since $C_{depl} < C_{ox}$ which allows to explain the measurements only down to ≈ 50 K. Including the interface-trap capacitance $C_{it} \propto qN_{it}$ (N_{it} is the number of interface states per unit area) in the slope factor ($m = m_0 + qN_{it}/C_{ox}$), does not help to model the behavior below ≈ 50 K, since this only further increases the linear slope of SS versus T .

Furthermore, this approach has led to unreasonably high N_{it} at deep-cryogenic temperatures. Typical N_{it} values that have been reported in the literature are in the order of $10^{13} - 10^{14}$ cm^{-2} at 4.2 K [16], [18], [19], and 10^{16} cm^{-2} at 20 mK [8]. The values at 4.2 K are still possible in principle. The values at 20 mK, however, exceed 7×10^{14} cm^{-2} corresponding to the number of atomic lattice sites per unit area in silicon. Furthermore, it should be emphasized that the Boltzmann limit leads to a singularity in N_{it} near 0 K.

Recently, relying on numerical simulations Bohuslavskyi *et al.* demonstrated that an exponential band tail and Fermi-Dirac statistics leads to saturation of SS at deep-cryogenic temperatures [32], [33].

The presence of a band tail in FDSOI FETs was explained by a combination of crystalline disorder, strain,

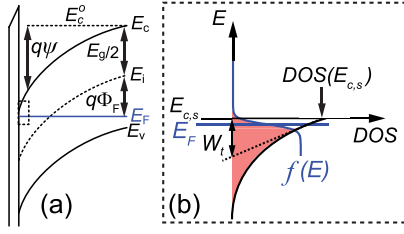


Fig. 2. (a) MOSFET band diagram with (b) a zoom-in on the band tail at the surface. W_t denotes the characteristic width of the exponential band tail, and $\psi \triangleq (E_c^o - E_c)/q$. Red area indicates the electron density.

residual impurities, etc. However, the saturation of $SS(T)$ has been measured in older technologies as well, before strain and nanometer dimensions were introduced that lead to disorder. Since $SS(T)$ is fairly independent of technology, this suggests that the extent of the band tail is fairly independent of technology, which points in the direction of an intrinsic mechanism being responsible for blurring the band edges (e.g., electron-phonon scattering, electron-electron and electron-hole interactions, finite crystalline periodicity, etc.) and to a lesser extent extrinsic mechanisms (impurities, disorder, defects, etc.) [34].

II. REVISED THEORETICAL LIMIT

The total drain current in subthreshold can be approximated by $I_{DS} = q(W/L)\mu(k_B T/q)(n_D - n_S)$, adopting the unified charge-controlled model that is valid for bulk, SOI, FinFET, and other multigate FETs including quantum effects [35]–[37] (q is the electron charge, W/L the width-over-length ratio of the transistor gate, μ the free-carrier mobility assumed constant along the channel, and n_D and n_S are the electron densities at the drain and source sides, assuming an n -channel FET without loss of generality). Hence, $SS = \partial V_{GS}/\partial \log I_{DS}$ can be expressed as $m[(n_D - n_S)/(\partial n_D/\partial \psi_s - \partial n_S/\partial \psi_s)] \ln 10$, where V_{GS} is the gate-to-source voltage, $m = \partial V_{GS}/\partial \psi_s = 1 + (C_{depl} + C_{it})/C_{ox}$, and ψ_s is the electrostatic potential at the surface compared to the bulk [Fig. 2(a)]. The electron density in a conduction-band tail [Fig. 2(b)] is described by:

$$n = \int_{-\infty}^{E_{c,s}} DOS(E_{c,s}) \exp\left(\frac{E - E_{c,s}}{W_t}\right) f(E) dE, \quad (1)$$

where $E_{c,s}$ is the conduction-band energy of the sharp band edge at the surface, W_t is the characteristic decay of an exponential band tail in the bandgap, and $f(E)$ is the Fermi-Dirac function. For simplicity, since SS will not depend on the exact value of $DOS(E_{c,s})$, we assume that $DOS(E_{c,s})$ can be given by the conduction-band DOS in 2-D: $N_c^{2D} = g_v m^*/(\pi \hbar^2)$, where $g_v = 2$ is the degeneracy factor, $m^* = 0.19 m_e$ is the effective mass in silicon (assumed temperature independent), m_e the electron mass, and \hbar the reduced Planck constant. The solution of integral (1) takes the form of a Gauss hypergeometric function (${}_2F_1 = F_1$) [38]:

$$n = N_c^{2D} W_t F_1(1, \theta; \theta + 1; z), \quad (2)$$

where $\theta = k_B T/W_t$, $z = -\exp[(E_{c,s} - E_{F,n})/(k_B T)]$ and $E_{F,n} = E_F - qV$ is the quasi-Fermi energy of electrons and V is the channel voltage. The band diagram in Fig. 2(a) shows that $E_F = E_c^o - E_g/2 - q\Phi_F$, where E_c^o is the conduction-band energy in thermal equilibrium, E_g the bandgap, and $\Phi_F = (k_B T/q) \ln(N_A/n_i)$ the Fermi potential with N_A the doping concentration in the MOSFET body and n_i the intrinsic carrier concentration.

The expression given for Φ_F assumes Boltzmann statistics, which has been verified at deep-cryogenic temperatures in case there is no band tail [29]. If a band tail is present, Fermi-Dirac statistics ought to be used like in (1) because the Fermi level can lie in the band tail which violates $E - E_{F,n} \gg 3k_B T$. In principle, the valence-band tail should be taken into account in the derivation of Φ_F . However, in the charge-neutrality condition in the p -type bulk ($p = N_A$), we can assume that there is no valence-band tail, hence Boltzmann statistics can be used to arrive at $\Phi_F = (k_B T/q) \ln(N_A/n_i)$. Including the valence-band tail in p would lead to a different value of Φ_F , which shifts the electron current, but does not change its slope. The same argument holds when dopant freezeout is included ($p = N_A^-$) [39]. For p -channel FETs, the roles of the conduction-band and valence-band tails would be reversed; the valence-band tail being responsible for the saturation of SS , and the conduction-band tail negligible in the computation of SS .

The bandgap is only slightly temperature dependent in the cryogenic regime [40]. Similar to a valence-band tail and dopant freezeout, bandgap widening will shift the electron current, but not change its slope.

Using $\psi_s \triangleq -(E_{c,s} - E_c^o)/q$, it follows that $E_{F,n} - E_{c,s} = q\psi_s - E_g/2 - q\Phi_F - qV$. The latter can be inserted in (2) to yield n as a function of ψ_s where $z = -\exp[-q\psi_s'/(k_B T)]$, $\psi_s' = \psi_s - \psi_s^*$, and $\psi_s^* = E_g/(2q) + \Phi_F + V$. The defined ψ_s^* depends only on T and N_A at a fixed V_{DS} . Note that for ψ_s in subthreshold, ranging from 0 (flatband) to $2\Phi_F + V$ (threshold), ψ_s' is always negative. The first derivative of a hypergeometric function $F_1(a, b; c; z)$ is given by $(ab/c)F_1(a+1, b+1; c+1; z)$ [41]. Differentiating (2) with respect to ψ_s (applying the chain rule for z), we find that

$$\frac{\partial n}{\partial \psi_s} = -qz N_c^{2D} \frac{F_1(2, \theta + 1; \theta + 2; z)}{\theta + 1}. \quad (3)$$

Inserting (2) and (3) in the expression for SS , gives:

$$SS = m \left(\frac{k_B T}{q} \right) \ln 10 \times A [z(\psi_s, V), T, W_t], \quad (4)$$

where A is given by

$$\frac{[\theta^{-1} F_1(1, \theta; \theta + 1; z)]_{V=0}^{V=V_{DS}}}{[-z(\theta + 1)^{-1} F_1(2, \theta + 1; \theta + 2; z)]_{V=0}^{V=V_{DS}}}. \quad (5)$$

Expression (4)-(5) is plotted in Fig. 3 versus T and ψ_s for different W_t together with the Boltzmann limit. As shown in Fig. 3, (i) SS rolls off from the Boltzmann limit and saturates at deep-cryogenic temperatures, (ii) the saturation value of SS increases with W_t , (iii) the critical temperature at which SS starts to deviate from the Boltzmann limit increases with W_t .

Expression (4)-(5) tends to the Boltzmann limit (i) at high temperatures ($k_B T \gg W_t$ or $\theta \rightarrow \infty$), and (ii) when the band-tail decay tends to zero ($W_t \rightarrow 0$ or $\theta \rightarrow \infty$). In both cases, $\theta \approx \theta + 1 \approx \theta + 2$ in (5). Using the relation $F_1(a, b; b; z) = (1 - z)^{-a}$ (which is valid for all b [41]) on both F_1 in (5), it follows that A tends to $(z - 1)/z$. Since ψ_s' in z is always negative in subthreshold, A tends to 1. The Boltzmann limit is then obtained in (4) for cases (i) and (ii).

Figures 4(a) and 4(b) show the measured transfer current characteristics in a large bulk silicon, n -channel MOSFET

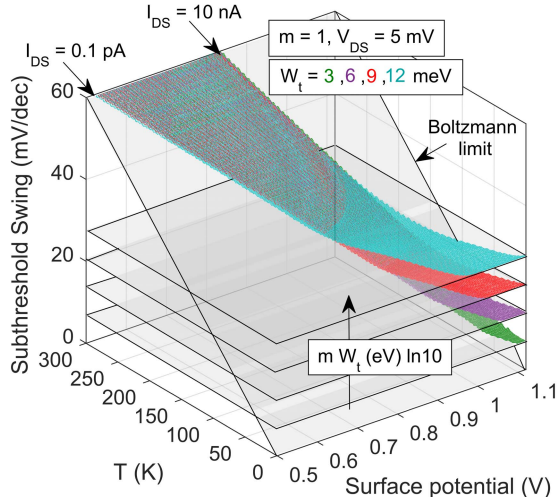


Fig. 3. Revised limit of SS (4)-(5) plotted for different W_t (colored surfaces). The range of surface potential ψ_s is limited to weak inversion (taken between the constant current values 0.1 pA and 10 nA). A linear increase in the electron mobility is assumed from $200 \text{ cm}^2\text{V}^{-1}\text{s}^{-1}$ at 300 K to $800 \text{ cm}^2\text{V}^{-1}\text{s}^{-1}$ at 1 K [4]. SS does not depend on the mobility. The mobility values are only used to compute the start and end ψ_s from $I_{DS} = 0.1 \text{ pA}$ and $I_{DS} = 10 \text{ nA}$. $W/L = 3$, and $N_A = 10^{17} \text{ cm}^{-3}$.

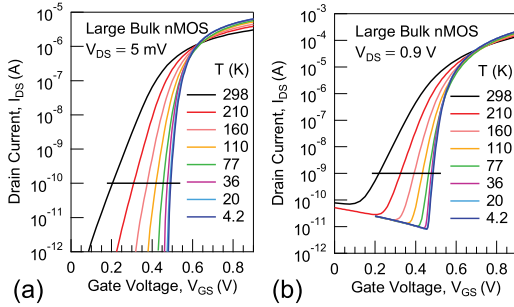


Fig. 4. Measured transfer characteristics down to 4.2 K in an n -channel, bulk-Si MOSFET with $W/L = 3 \mu\text{m}/1 \mu\text{m}$ from a commercial 28-nm bulk CMOS process, a) at low V_{DS} and b) high V_{DS} . Horizontal lines indicate current levels at which SS was extracted and shown in Fig. 1.

from 298 K down to 4.2 K and biased at low and high V_{DS} , respectively. The device was fabricated in a commercial 28-nm bulk CMOS process. The measurements were performed using a Lakeshore CPX cryogenic probe station and a Keysight B1500a semiconductor device analyzer. In Fig. 5, the derived limit is successfully compared with the measurements from Fig. 4(a) at low V_{DS} . The extracted value of W_t lies within the range of possible band-tail decays measured by electron-spin resonance in silicon FETs at sub-Kelvin temperatures [42]. Note that SS at 300 K in Fig. 5 is not affected by the band tail. A slope factor of $m = 1.1$ is assumed for bulk technology (doping and traps).

III. SATURATION VALUE

An expression for the saturation value of SS at deep cryogenic temperatures ($k_B T \ll W_t$ or $\theta \rightarrow 0$) can be derived from (4)-(5):

$$SS^{k_B T \ll W_t} = m \left(\frac{W_t}{q} \right) \ln 10 \times \frac{F_1(1, 0; 1; z)}{F_1(2, 1; 2; z)} (-z)^{-1} \quad (6)$$

where W_t is in Joules. Applying one of Euler's linear transformations for hypergeometric functions,

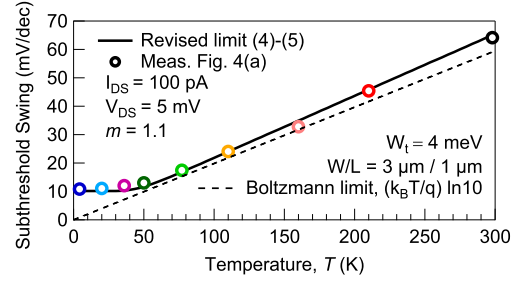


Fig. 5. Experimental validation of the revised SS limit from (4)-(5).

i.e., $F_1(a, b; c; z) = (1 - z)^{-b} F_1(b, c - a; c; z')$ [41], where $|z'| = |z/(z - 1)| < 1$ and $c = a$, gives

$$SS^{k_B T \ll W_t} = m \left(\frac{W_t}{q} \right) \ln 10 \times \frac{F_1(0, 0; 1; z')}{F_1(1, 0; 2; z')} (1 - z')^{-1} \quad (7)$$

The hypergeometric functions in the numerator and denominator of (7) are both equal to one, because either a or b is zero in the series representation [41]. Since ψ'_s is negative and $k_B T$ small, $z^{-1} \rightarrow 0$, we obtain a saturation value that is independent of T , ψ_s , and V_{DS} , and proportional to W_t :

$$SS^{k_B T \ll W_t} = m \left(\frac{W_t}{q} \right) \ln 10 \quad (8)$$

The above result confirms the saturation value of SS that was apparent in the numerical simulations by Bohuslavskyi *et al.* [32], [33]. The revised limit in (4)-(5) and saturation value in (8) are valid for bulk, SOI, FinFET, nanowire, and other multigate FETs, provided that m accounts for enhanced electrostatic control. The horizontal planes in Fig. 3 indicate the saturation values for increasing W_t . The critical temperature for which SS deviates from the Boltzmann limit can be estimated as $T_{crit} = W_t/k_B$. In Fig. 5, T_{crit} is about 46 K. Similarly, T_{crit} provides a simple method to obtain W_t from dc measurements by plotting SS versus T . Furthermore, (8) demonstrates that the deep-cryogenic subthreshold performance of FETs is determined by W_t and N_{it} (in m). A more reasonable N_{it} can be extracted at sub-Kelvin temperatures by using (8) instead of the Boltzmann limit. The singularity of N_{it} near 0 K is also avoided. Since (8) is independent of V_{DS} , the slightly higher SS in Fig. 1 at $V_{DS} = 0.9 \text{ V}$ compared to $V_{DS} = 5 \text{ mV}$ is a high-field effect.

IV. CONCLUSION

An analytical expression for the saturating SS(T) is derived from room down to sub-Kelvin temperature. When the thermal energy becomes smaller than the band-tail extension (W_t), the revised SS(T) limit follows the temperature-independent $m(W_t/q) \ln 10$ rather than $m(k_B T/q) \ln 10$. The revised limit demonstrates that a perfect MOS switch ($SS = 0$) cannot be obtained in the presence of a band tail. The problem of extracting anomalously high interface-trap density at deep-cryogenic temperatures is solved by using $m(W_t/q) \ln 10$.

REFERENCES

- [1] A. Kamgar, "Subthreshold behavior of silicon MOSFETs at 4.2 K," *Solid-State Electron.*, vol. 25, no. 7, pp. 537–539, Jul. 1982.
- [2] I. M. Hafez, G. Ghibardo, and F. Balestra, "Assessment of interface state density in silicon metal-oxide-semiconductor transistors at room, liquid-nitrogen, and liquid-helium temperatures," *J. Appl. Phys.*, vol. 67, no. 4, pp. 1950–1952, Feb. 1990.

- [3] F. Balestra and G. Ghibaudo, "Physics and performance of nanoscale semiconductor devices at cryogenic temperatures," *Semicond. Sci. Technol.*, vol. 32, no. 2, Feb. 2017, Art. no. 023002.
- [4] A. Beckers, F. Jazaeri, A. Ruffino, C. Bruschini, A. Baschiroto, and C. Enz, "Cryogenic characterization of 28 nm bulk CMOS technology for quantum computing," in *Proc. 47th Eur. Solid-State Device Res. Conf. (ESSDERC)*, Sep. 2017, pp. 62–65.
- [5] A. Beckers, F. Jazaeri, and C. Enz, "Characterization and modeling of 28-nm bulk CMOS technology down to 4.2 K," *IEEE J. Electron Devices Soc.*, vol. 6, pp. 1007–1018, Mar. 2018.
- [6] H. Homulle, L. Song, E. Charbon, and F. Sebastiano, "The cryogenic temperature behavior of bipolar, MOS, and DTMOs transistors in standard CMOS," *IEEE J. Electron Devices Soc.*, vol. 6, pp. 263–270, Jan. 2018.
- [7] R. M. Incandela, L. Song, H. Homulle, E. Charbon, A. Vladimirescu, and F. Sebastiano, "Characterization and compact modeling of nanometer CMOS transistors at deep-cryogenic temperatures," *IEEE J. Electron Devices Soc.*, vol. 6, pp. 996–1006, Apr. 2018.
- [8] P. Galy, J. Camirand Lemyre, P. Lemieux, F. Arnaud, D. Drouin, and M. Pioro-Ladriere, "Cryogenic temperature characterization of a 28-nm FD-SOI dedicated structure for advanced CMOS and quantum technologies co-integration," *IEEE J. Electron Devices Soc.*, vol. 6, pp. 594–600, May 2018.
- [9] E. A. Gutierrez-D, J. Deen, and C. Claeys, *Low Temperature Electronics: Physics, Devices, Circuits, and Applications*. Amsterdam, The Netherlands: Elsevier, 2000.
- [10] F. Balestra and G. Ghibaudo, *Device Circuit Cryogenic Operation For Low Temperature Electronics*. New York, NY, USA: Springer, 2001.
- [11] T. Elewa, F. Balestra, S. Cristoloveanu, I. Hafez, J.-P. Colinge, A.-J. Auberton-Herve, and J. Davis, "Performance and physical mechanisms in SIMOX MOS transistors operated at very low temperature," *IEEE Trans. Electron Devices*, vol. 37, no. 4, pp. 1007–1019, Apr. 1990.
- [12] M. Shin, M. Shi, M. Mouis, A. Cros, E. Josse, G. T. Kim, and G. Ghibaudo, "Low temperature characterization of 14 nm FDSOI CMOS devices," in *Proc. 11th Int. Workshop Low Temp. Electron. (WOLTE)*, Jul. 2014, pp. 29–32.
- [13] H. Bohuslavskiy, S. Barraud, M. Cassé, V. Barrau, B. Bertrand, L. Hutin, F. Arnaud, P. Galy, M. Sanquer, S. De Franceschi, and M. Vinet, "28 nm Fully-depleted SOI technology: Cryogenic control electronics for quantum computing," in *Proc. Silicon Nanoelectronics Workshop (SNW)*, Jun. 2017, pp. 143–144.
- [14] A. Beckers, F. Jazaeri, H. Bohuslavskiy, L. Hutin, S. De Franceschi, and C. Enz, "Characterization and modeling of 28-nm FDSOI CMOS technology down to cryogenic temperatures," *Solid-State Electron.*, vol. 159, pp. 106–115, Sep. 2019.
- [15] H. Achour, R. Talmat, B. Cretu, J.-M. Routoure, A. Benfdila, R. Carin, N. Collaert, E. Simoen, A. Mercha, and C. Claeys, "DC and low frequency noise performances of SOI p-FinFETs at very low temperature," *Solid-State Electron.*, vol. 90, pp. 160–165, Dec. 2013.
- [16] B. Cretu, D. Boudier, E. Simoen, A. Veloso, and N. Collaert, "Assessment of DC and low-frequency noise performances of triple-gate FinFETs at cryogenic temperatures," *Semicond. Sci. Technol.*, vol. 31, no. 12, Dec. 2016, Art. no. 124006.
- [17] D. Boudier, B. Cretu, E. Simoen, A. Veloso, and N. Collaert, "Detailed characterisation of Si gate-all-around nanowire MOSFETs at cryogenic temperatures," *Solid-State Electron.*, vol. 143, pp. 27–32, May 2018.
- [18] R. Trevisoli, M. De Souza, R. T. Doria, V. Kilchtyaska, D. Flandre, and M. A. Pavanello, "Effect of the temperature on on junctionless nanowire transistors electrical parameters down to 4K," in *Proc. 29th Symp. Microelectron. Technol. Devices (SBMicro)*, Sep. 2014, pp. 1–4.
- [19] R. Trevisoli, M. De Souza, R. T. Doria, V. Kilchtyaska, D. Flandre, and M. A. Pavanello, "Junctionless nanowire transistors operation at temperatures down to 4.2 K," *Semicond. Sci. Technol.*, vol. 31, no. 11, Nov. 2016, Art. no. 114001.
- [20] B. C. Paz, M. A. Pavanello, M. Cassé, S. Barraud, G. Reimbold, M. Vinet, and O. Faynot, "Cryogenic operation of Ω -gate p-type SiGeon-insulator nanowire MOSFETs," in *Proc. Joint Int. EUROSIOI Workshop Int. Conf. Ultimate Integr. Silicon (EUROSIOI-ULIS)*, Mar. 2018, pp. 1–4.
- [21] J. Schlee, H. Rodilla, N. Wadefalk, P. Nilsson, and J. Grahn, "Characterization and modeling of cryogenic ultralow-noise InP HEMTs," *IEEE Trans. Electron Devices*, vol. 60, no. 1, pp. 206–212, Jan. 2013.
- [22] T. Kobayashi, S. Nakazawa, T. Okuda, J. Suda, and T. Kimoto, "Interface state density of SiO₂/p-type 4H-SiC (0001), (1120), (1100) metal-oxide-semiconductor structures characterized by low-temperature subthreshold slopes," *Appl. Phys. Lett.*, vol. 108, no. 15, Apr. 2016, Art. no. 152108, doi: 10.1063/1.4946863.
- [23] J. J. Pla, K. Y. Tan, J. P. Dehollain, W. H. Lim, J. J. L. Morton, D. N. Jamieson, A. S. Dzurak, and A. Morello, "A single-atom electron spin qubit in silicon," *Nature*, vol. 489, no. 7417, pp. 541–545, Sep. 2012.
- [24] J. J. L. Morton, D. R. McCamey, M. A. Eriksson, and S. A. Lyon, "Embracing the quantum limit in silicon computing," *Nature*, vol. 479, no. 7373, pp. 345–353, Nov. 2011.
- [25] R. Maurand, X. Jehl, D. Kotekar-Patil, A. Corna, H. Bohuslavskiy, R. Laviéville, L. Hutin, S. Barraud, M. Vinet, M. Sanquer, and S. De Franceschi, "A CMOS silicon spin qubit," *Nature Commun.*, vol. 7, Nov. 2016, Art. no. 13575, doi: 10.1038/ncomms13575.
- [26] L. Vandersypen, H. Bluhm, J. Clarke, A. Dzurak, R. Ishihara, A. Morello, D. Reilly, L. Schreiber, and M. Veldhorst, "Interfacing spin qubits in quantum dots and donors—hot, dense, and coherent," *npj Quantum Inf.*, vol. 3, no. 1, p. 34, Sep. 2017.
- [27] E. Charbon, F. Sebastiano, A. Vladimirescu, H. Homulle, S. Visser, L. Song, and R. M. Incandela, "Cryo-CMOS for quantum computing," in *IEDM Tech. Dig.*, Dec. 2016, pp. 13.5.1–13.5.4.
- [28] S. Schaal, A. Rossi, V. N. Ciriano-Tejel, T.-Y. Yang, S. Barraud, J. J. L. Morton, and M. F. Gonzalez-Zalba, "A CMOS dynamic random access architecture for radio-frequency readout of quantum devices," *Nature Electron.*, vol. 2, no. 6, pp. 236–242, Jun. 2019.
- [29] A. Beckers, F. Jazaeri, and C. Enz, "Cryogenic MOS transistor model," *IEEE Trans. Electron Devices*, vol. 65, no. 9, pp. 3617–3625, Sep. 2018.
- [30] F. Jazaeri, A. Beckers, A. Tajalli, and J.-M. Sallese, "A review on quantum computing: From qubits to front-end electronics and cryogenic MOSFET physics," in *Proc. 26th Int. Conf. Mixed Des. Integr. Circuits Syst. (MIXDES)*, Jun. 2019, pp. 15–25.
- [31] M. J. Deen, "Cryogenic operation of CMOS-based microsystems and computers," *Microprocessors Microsyst.*, vol. 13, no. 4, pp. 245–253, May 1989. [Online]. Available: <http://www.sciencedirect.com/science/article/pii/0141933189900628>
- [32] H. Bohuslavskiy, A. G. M. Jansen, S. Barraud, V. Barrau, M. Cassé, L. Le Guevel, X. Jehl, L. Hutin, B. Bertrand, G. Billiot, G. Pillonnet, F. Arnaud, P. Galy, S. De Franceschi, M. Vinet, and M. Sanquer, "Cryogenic subthreshold swing saturation in FD-SOI MOSFETs described with band broadening," *IEEE Electron Device Lett.*, vol. 40, no. 5, pp. 784–787, May 2019.
- [33] H. Bohuslavskiy, "Cryogenic electronics and quantum dots on silicon-insulator for quantum computing," Ph.D. dissertation, Laboratoire d'Electronique et de Technologie de l'Information, Communauté Université Grenoble Alpes, Gières, France, 2016, ch. 4.
- [34] P. Sarangapani, Y. Chu, J. Charles, G. Klimeck, and T. Kubis, "Band-tail formation and band-gap narrowing driven by polar optical phonons and charged impurities in atomically resolved III-V semiconductors and nanodevices," *Phys. Rev. Appl.*, vol. 12, Oct. 2019, Art. no. 044045, doi: 10.1103/PhysRevApplied.12.044045.
- [35] C.-K. Park, C.-Y. Lee, K. Lee, B.-J. Moon, Y. H. Byun, and M. Shur, "A unified current-voltage model for long-channel nMOSFETs," *IEEE Trans. Electron Devices*, vol. 38, no. 2, pp. 399–406, Feb. 1991.
- [36] T. Rudenko, A. Nazarov, V. Kilchtyaska, and D. Flandre, "A review of special gate coupling effects in long-channel SOI MOSFETs with lightly doped ultra-thin bodies and their compact analytical modeling," *Solid-State Electron.*, vol. 117, pp. 66–76, Mar. 2016. [Online]. Available: <http://www.sciencedirect.com/science/article/pii/S0038110115003366>
- [37] Y. Taur and T. H. Ning, *Fundamentals of Modern VLSI Devices*, 2nd ed. Cambridge, U.K.: Cambridge Univ. Press, 2009.
- [38] L. C. Andrews, *Special Functions of Mathematics for Engineers*. London, U.K.: Oxford Univ. Press, 1997, pp. 357–363, ch. 9.
- [39] A. Beckers, F. Jazaeri, and C. Enz, "Cryogenic MOSFET threshold voltage model," in *Proc. 49th Eur. Solid-State Device Res. Conf. (ESSDERC)*, Sep. 2019, pp. 94–97.
- [40] Y. P. Varshni, "Temperature dependence of the energy gap in semiconductors," *Physica*, vol. 34, no. 1, pp. 149–154, Jan. 1967. [Online]. Available: <http://www.sciencedirect.com/science/article/pii/0031891467900626>
- [41] M. Abramowitz and I. A. Stegun, *Handbook of Mathematical Functions with Formulas, Graphs, and Mathematical Tables*. New York, NY, USA: Dover, 1968, pp. 555–559, ch. 15.
- [42] R. M. Jock, S. Shankar, A. M. Tyryshkin, J. He, K. Eng, K. D. Childs, L. A. Tracy, M. P. Lilly, M. S. Carroll, and S. A. Lyon, "Probing band-tail states in silicon metal-oxide-semiconductor heterostructures with electron spin resonance," *Appl. Phys. Lett.*, vol. 100, no. 2, Jan. 2012, Art. no. 023503, doi: 10.1063/1.3675862.